

Supporting Information

Truncated concave octahedral Cu₂O nanocrystals with {*hkk*} high-index facets for enhanced activity and stability in heterogeneous catalytic azide-alkyne cycloaddition

Zelun Zhao,^{ab} Xue Wang,^{*a} Jiaqi Si,^a Chengtao Yue,^{ab} Chungu Xia,^a and Fuwei Li^{*ac}

^aState Key Laboratory for Oxo Synthesis and Selective Oxidation, Suzhou Research Institute of LICP, Lanzhou Institute of Chemical Physics (LICP), Chinese Academy of Sciences, Lanzhou 730000, China.

^bUniversity of the Chinese Academy of Sciences, Beijing 100049, China

^cSchool of Material Science and Engineering, Guilin University of Electronic Technology, Guilin 541004, China

Corresponding authors: xuewang@licp.cas.cn; fuweili@licp.cas.cn

Experimental Section

Materials

Copper(II) sulfate pentahydrate ($\text{CuSO}_4 \cdot 5\text{H}_2\text{O}$, $\geq 99\%$), sodium hydroxide (NaOH , $\geq 96\%$), Sodium ascorbate (SA, 99%), potassium hydroxide (KOH , 95%), and sulfuric acid (H_2SO_4 , 98%) were purchased from Sinopharm Chemical Reagent Co., Ltd. Benzyl azide (97%), 1-(azidomethyl)-3-methoxybenzene (98%), and a series of alkynes (1-hexyne, 97%; 3-ethynyltoluene, 4-ethynyltoluene, 98%; 3-chlorophenylacetylene, 97%; 4-chlorophenylacetylene, 98%; 4-fluorophenylacetylene, 98%; phenylacetylene, 98%) were purchased from J&K Scientific Ltd. Oleic acid (OA, 90%) was obtained from Alfa Aesar Chemicals Co., Ltd. All the chemicals were used as received without further purification. The aqueous solutions were prepared with DI water (18.2 M Ω cm).

Synthesis

For the synthesis of Cu_2O truncated concave octahedral nanocrystals, firstly, 0.1 M of aqueous solution of CuSO_4 (1 ml), DI water (6.7 mL), and oleic acid (0.5 mL) were added in a vial. The solution then was separated into two phases with water phase on the bottom and oil phase on top. The solution was stirred in a water bath of 50 °C. When oil phase turned blue, 1.0 M of aqueous solution of NaOH (1.3 mL) was added quickly. After stirring for 15 minutes, the solution turned into emulsion with blue color and 0.1 M of aqueous solution of SA (1 mL) was added into the solution. The vial was kept in water bath for another 60 minutes with constant stirring. The product was collected by centrifugation at 6,000 rpm and washed nine times with ethanol and hexane. Finally the product was vacuum dried at room temperature for further use.

The synthesis methods of Cu_2O rhombic dodecahedral and cubic nanocrystals were similar to that of Cu_2O truncated concave octahedral nanocrystals. By adjusting the amount of NaOH solution (1.0 M) to 1.05 and 1.85 mL, respectively, rhombic dodecahedra and cubes could be obtained.

Instrumental analysis

The morphologies of the as-prepared samples were observed by scanning electron microscopy (SEM, S4800). TEM images and SAED patterns were obtained using a FEI F20 with an acceleration voltage of 200 kV. XRD patterns were recorded on a Bruker D8 diffractometer with $\text{Cu-K}\alpha$ radiation. The surface areas of samples were measured by BET method on a Micrometrics ASAP 2020 HD88 system. The ζ potential measurements were performed on a

Malvern ZS90. The concentration of Cu in reaction solution was measured by ICP-MS (NEXION 300D). ^1H NMR and ^{13}C NMR spectra were operated at 400 and 100 MHz, respectively. Tetramethylsilane and chloroform-d (CDCl_3) were used as internal standard for ^1H NMR and ^{13}C NMR spectra, respectively. The pH values of solution were measured by a pH meter (PHS-3C, INESA Scientific Instrument Co., Ltd). FT-IR spectra were performed on a Thermo Fisher Scientific Nicolet 6700 spectrometer. The surface composition analyses of samples were performed on a Thermo Fisher Scientific K-Alpha X-ray photoelectron spectrometer.

Carbon monoxide temperature programmed desorption (CO-TPD) tests

CO-TPD measurements were achieved on a XIANQUAN TP-5080 instrument (Tianjin, China). Typically, 31.5 mg of Cu_2O nanocrystals with different morphologies were pretreated at 80 °C for 1 h in helium flow (30 mL min^{-1}). Then the temperature decreased to 50 °C, and 10% CO in He (30 mL min^{-1}) was fed continually for 1 h. Subsequently, helium was blown for 30 min to remove unadsorbed CO. The process of CO desorption was performed from 50 to 350 °C at a heating rate of 10 °C min^{-1} in helium (30 mL min^{-1}). The TCD signals were recorded online. The CO adsorption amount was calculated by integrating the CO-TPD profiles. As there is a liner correlation between the amount of Cu(I) on surface and the adsorbed amount of CO,^{1,2} the amount of Cu(I) was calculated based on the amount of adsorbed CO.

Cu_2O nanocatalysts catalyzed azide-alkyne cycloaddition

The catalysis activities of Cu_2O nanocrystals with different morphologies toward azide-alkyne cycloaddition were measured. Typically, benzyl azide (0.25 mmol), alkyne (0.25 mmol), 1 mL of DI water, and 2 mg (13.9 μmol) of Cu_2O catalyst were added into a sealed glass reactor. Air in the reactor was removed by purging with N_2 for three times. The reaction was performed at 40 °C for different reaction times with a stirring speed of 300 rpm. When the reaction was stopped, 8 mL of ethanol was added immediately to dissolve the products. Catalyst and solution were separated by centrifugation at 8,000 rpm for 5 min. The separated catalysts were washed with ethanol three times and vacuum dried at room temperature for further use.

The solution was evenly divided into two parts for identification and quantification of product, respectively. The product was identified by NMR spectra. Typically, the solvent in solution was removed through reduced pressure distillation, and then water and dichloromethane were added to extract the product twice. The dichloromethane layer was dried with anhydrous MgSO_4 . After filtration, the obtained solution was evaporated to get crude product. The crude

product was dissolved in 2 mL ethyl acetate and purified by silica gel plate with mixture solution of ethyl acetate and petroleum ether ($V_{\text{ethyl acetate}} : V_{\text{petroleum ether}} = 1:9$) as eluent. The purified product was dissolved in CDCl_3 solution containing 0.03% tetramethylsilane and identified by NMR spectra.

Another half solution was used to quantify the product using high performance liquid chromatography (HPLC, Agilent 1200) with a C18 column and ultraviolet detector by external standard method. The mobile phase of HPLC was a mixture solution of water and acetonitrile with the volume ratio of 9:11.

TOF calculation

The TOF was calculated on the basis of BPT yields below 20% according to the equation (1). For truncated concave octahedra, rhombic dodecahedra, and cubes, we calculated TOF based on BPT yield of 18.0% at 10 min, 15.5% at 15 min, and 16.6% at 45 min, respectively. The m_{BPT} (g) and M_{BPT} (g mol^{-1}) are the mass and molar mass of obtained BPT, respectively. The $\rho_{\text{Cu(I)}}$ (%) is the mole percentage of surface Cu(I) over the total Cu(I) in the Cu_2O catalyst, which could be determined by carbon monoxide temperature programmed desorption (Table S4†). The $m_{\text{Cu}_2\text{O}}$ (g) and $M_{\text{Cu}_2\text{O}}$ (g mol^{-1}) are the mass and molar mass of Cu_2O catalysts, respectively. The t (h) is the reaction time.

$$TOF = \frac{m_{\text{BPT}}/M_{\text{BPT}}}{\rho_{\text{Cu(I)}} \times (m_{\text{Cu}_2\text{O}}/M_{\text{Cu}_2\text{O}} \times 2) \times t} \quad (1)$$

Recyclability of Cu_2O truncated concave octahedra for azide-alkyne cycloaddition

The separated Cu_2O catalyst was dispersed in 1 mL of DI water, followed by adding benzyl azide (0.25 mmol) and phenylacetylene (0.25 mmol). The reaction then was conducted at 40 °C for a period of time with stirring under N_2 . Catalyst separation and product detection was done according to the above procedure. The separated catalysts were further washed and vacuum dried for the next catalytic cycle.

References

- (1) M. Davidová, D. Nachtigallová, R. Bulánek and P. Nachtigall, *J. Phys. Chem. B*, 2003, **107**, 2327-2332.

- (2) H. Chen, M. Matsuoka, J. Zhang and M. Anpo, *J. Phys. Chem. B*, 2006, **110**, 4263-4269.
- (3) M. C. Biesinger, L. W. M. Lau, A. R. Gerson and R. S. C. Smart, *Appl. Surf. Sci.*, 2010, **257**, 887-898.
- (4) A. Radi, D. Pradhan, Y. Sohn and K. T. Leung, *ACS Nano*, 2010, **4**, 1553-1560.
- (5) A. Adenot, E. B. Landstorm, F. Gallou and B. H. Lipshutz, *Green Chem.*, 2017, **19**, 2506-2509.
- (6) B. J. Borah, D. Dutta, P. P. Saikia, N. C. Barua and D. K. Dutta, *Green Chem.*, 2011, **13**, 3453-3460.
- (7) F. Fu, A. Martinez, C. Wang, R. Ciganda, L. Yate, A. Escobar, S. Moya, E. Fouquet, J. Ruiz and D. Astruc, *Chem. Commun.*, 2017, **53**, 5384-5387.
- (8) D. Clarisse, P. Prakash, V. Geertsen, F. Miserque, E. Gravel and E. Doris, *Green Chem.*, 2017, **19**, 3112-3115.
- (9) K. Wang, X. Bi, S. Xing, P. Liao, Z. Fang, X. Meng, Q. Zhang, Q. Liu and Y. Ji, *Green Chem.*, 2011, **13**, 562-565.
- (10) N. Mukherjee, S. Ahammed, S. Bhadra and B. C. Ranu, *Green Chem.*, 2013, **15**, 389-397.
- (11) K. Chanda, S. Rej and M. H. Huang, *Chem. Eur. J.*, 2013, **19**, 16036-16043.
- (12) Y.-H. Tsai, K. Chanda, Y.-T. Chu, C.-Y. Chiu and M. H. Huang, *Nanoscale*, 2014, **6**, 8704-8709.

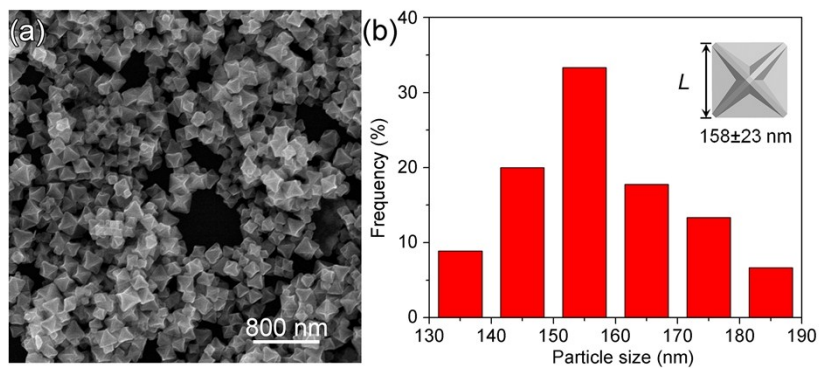


Fig. S1 (a) SEM image of truncated concave octahedral Cu_2O nanocrystals prepared by standard method and (b) the corresponding particle size distribution histogram. The particle size was measured according to the length L (inset) of a Cu_2O nanocrystal.

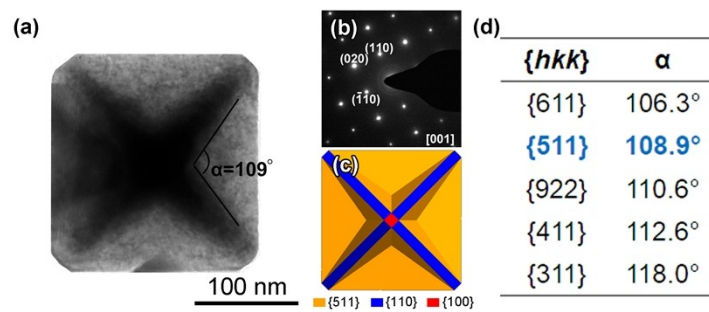


Fig. S2 (a) TEM image, (b) the corresponding SAED pattern, and (c) schematic model of a truncated concave octahedron exposed with $\{511\}$, $\{100\}$ and $\{110\}$ facets, projected along $[001]$ direction. (d) $\{hkk\}$ facets of truncated concave octahedron and the corresponding projection angles α .

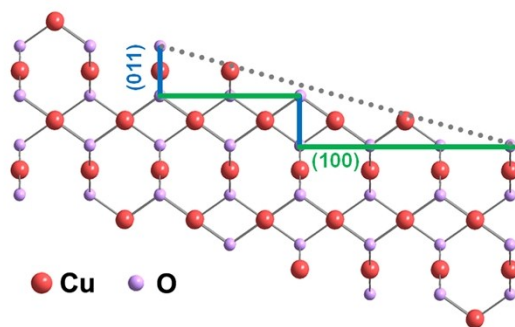


Fig. S3 Schematic model of Cu₂O (511) surface projected along $[0\bar{1}1]$ direction. (511) surface can be seen as a combination of five (100) terraces (green line) and one (011) step (blue line).

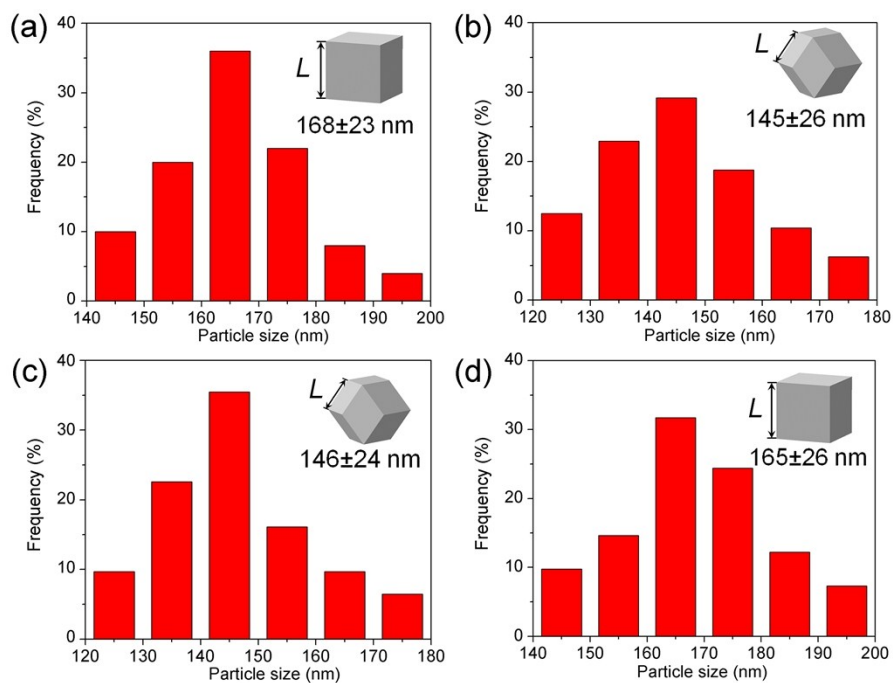


Fig. S4 Particle size distribution histograms of (a) Cu_2O cubic nanocrystals in Fig. 2b, (b) Cu_2O rhombic dodecahedral nanocrystals in Fig. 2c, (c) Cu_2O rhombic dodecahedral nanocrystals in Fig. 3a, and (d) Cu_2O cubic nanocrystals in Fig. 3b. The particle sizes were measured according to the edge length L (insets) of the corresponding Cu_2O nanocrystals.

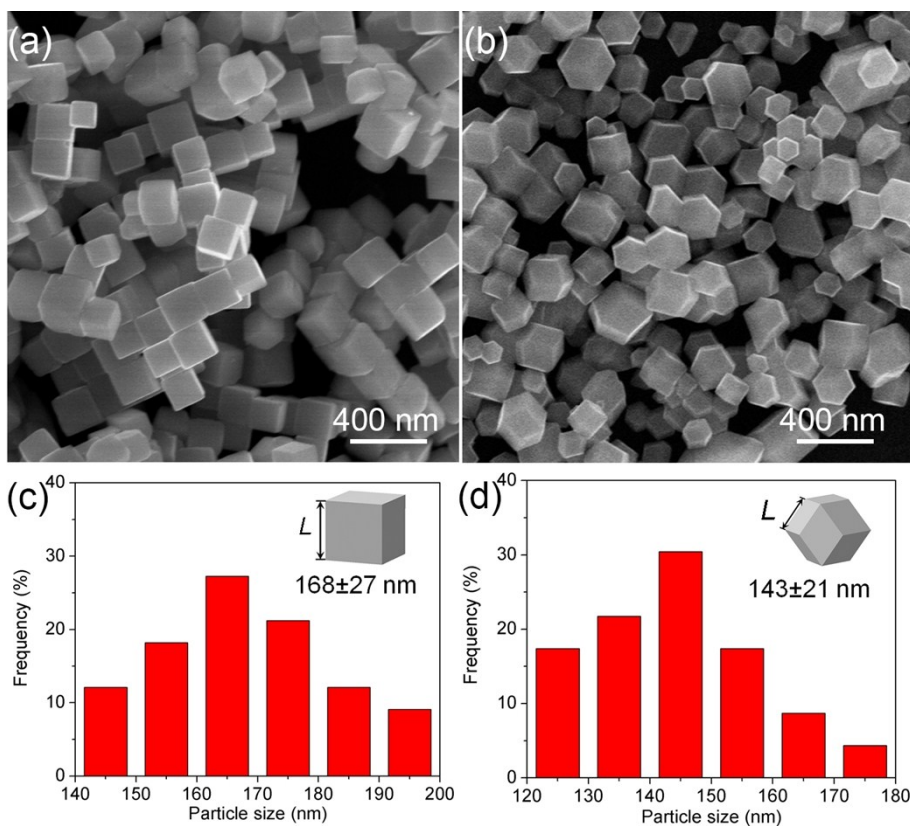


Fig. S5 SEM images of Cu₂O nanocrystals synthesized using the standard method for Cu₂O truncated concave octahedra, except for adding additional reagents: (a) 0.55 mL of KOH (1.0 M) and (b) 58 μ L of H₂SO₄ (2.0 M). Particle size distribution histograms of (c) Cu₂O cubic nanocrystals in Fig. S5a, and (d) Cu₂O rhombic dodecahedral nanocrystals in Fig. S5b. The particle sizes were measured according to the edge length L (insets) of the corresponding Cu₂O nanocrystals.

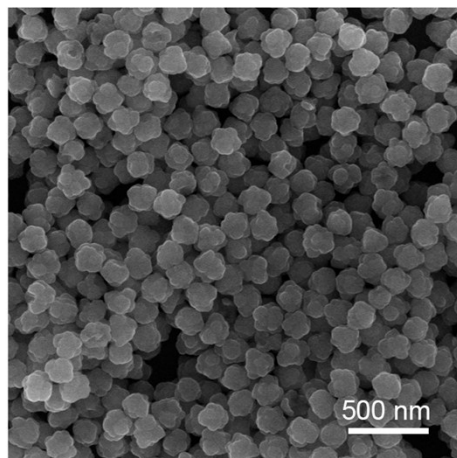


Fig. S6 SEM image of Cu₂O nanoparticles prepared by the standard method for Cu₂O truncated concave octahedra, except for adjusting the amount of 1.0 M NaOH solution to keep the synthetic solution with pH=9.0 in the absence of oleic acid.

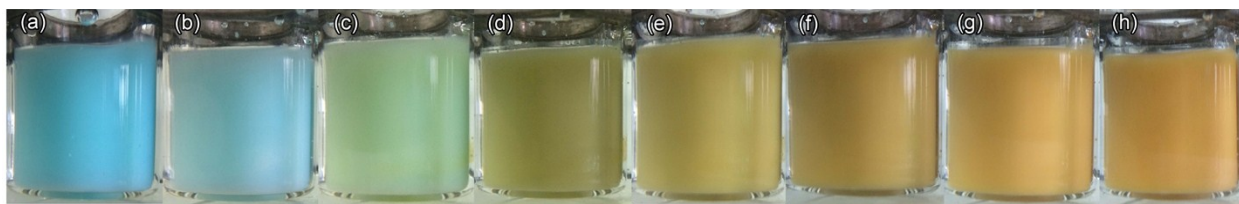


Fig. S7 Photographs showing the color change of the solution as a function of reaction time during synthesis of Cu_2O rhombic dodecahedral nanocrystals in Fig. 3a. (a) 5 s, (b) 10 min, (c) 20 min, (d) 30 min, (e) 35 min, (f) 40 min, (g) 50 min, and (h) 60 min after adding sodium ascorbate.

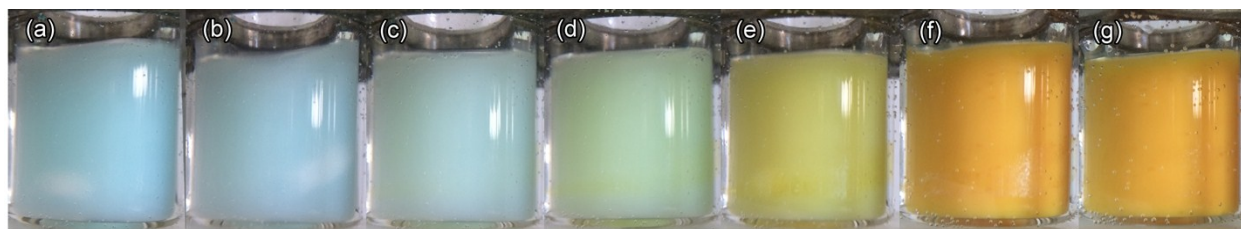


Fig. S8 Photographs showing the color change of the solution as a function of reaction time during synthesis of Cu_2O truncated concave octahedral nanocrystals in Fig. 1a. (a) 5 s, (b) 60 s, (c) 3 min, (d) 5 min, (e) 10 min, (f) 30 min, and (g) 60 min after adding sodium ascorbate.



Fig. S9 Photographs showing the color change of the solution as a function of reaction time during synthesis of Cu_2O cubic nanocrystals in Fig. 3b. (a) 5 s, (b) 10 s, (c) 15 s, (d) 20 s, (e) 30 s, (f) 60 s, (g) 5 min, and (h) 60 min after adding sodium ascorbate.

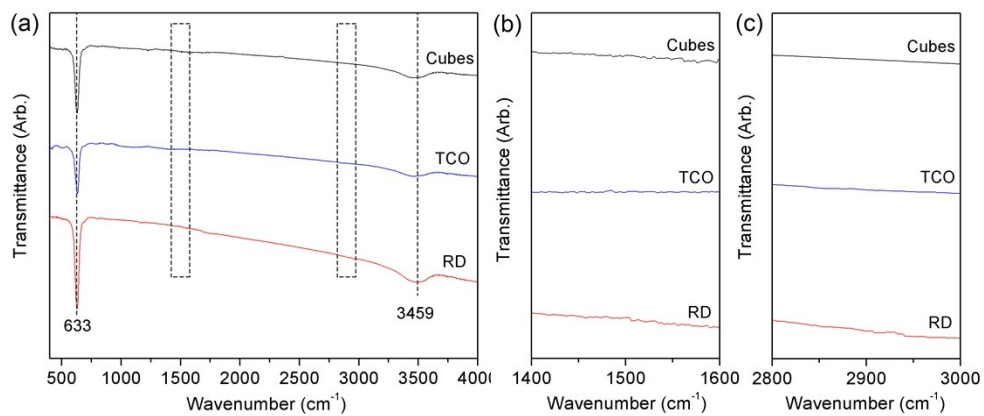


Fig. S10 (a) FT-IR spectra of Cu₂O cubic, truncated concave octahedral (TCO), and rhombic dodecahedral (RD) nanocrystals. (b) An enlarge view of the section from 1400 to 1600 cm⁻¹. (c) An enlarge view of the section from 2800 to 3000 cm⁻¹.

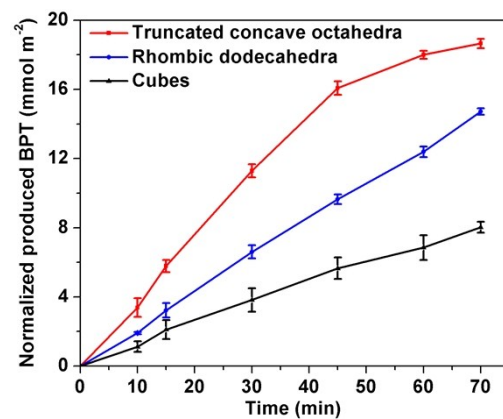


Fig. S11 The amounts of produced BPT catalyzed by Cu₂O cubes, truncated concave octahedra, and rhombic dodecahedra at 40 °C for different reaction times, which was normalized with their surface areas. Error bars refer to the standard deviation based on three repeated experiments.

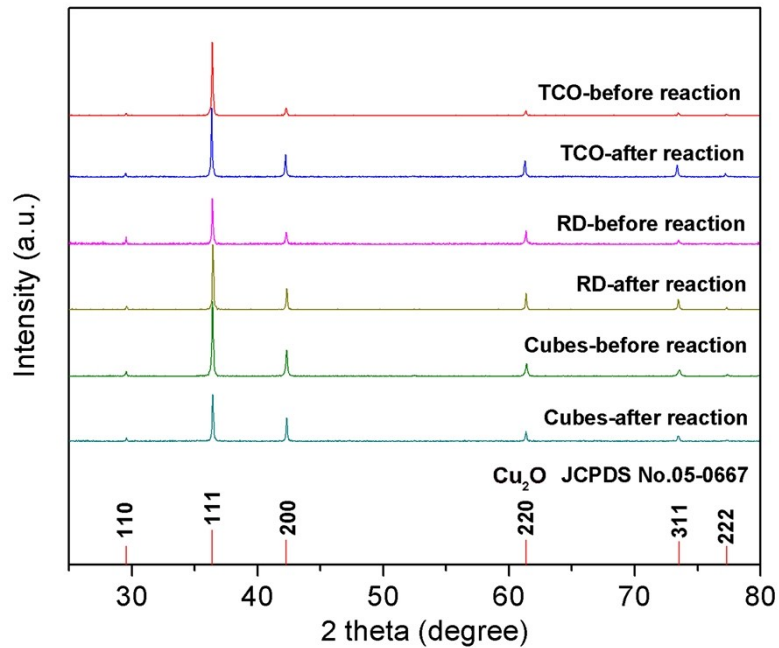


Fig. S12 XRD patterns of Cu₂O nanocrystals with different morphologies of truncated concave octahedra (TCO), rhombic dodecahedra (RD), and cubes before and after catalytic reaction.

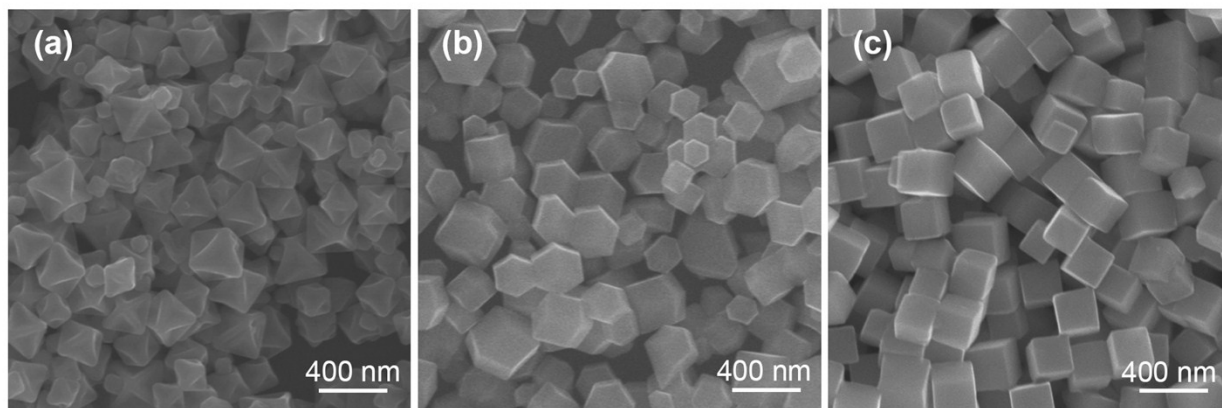


Fig. S13 SEM images of Cu_2O nanocrystals after catalytic reaction: (a) truncated concave octahedra, (b) rhombic dodecahedra, and (c) cubes.

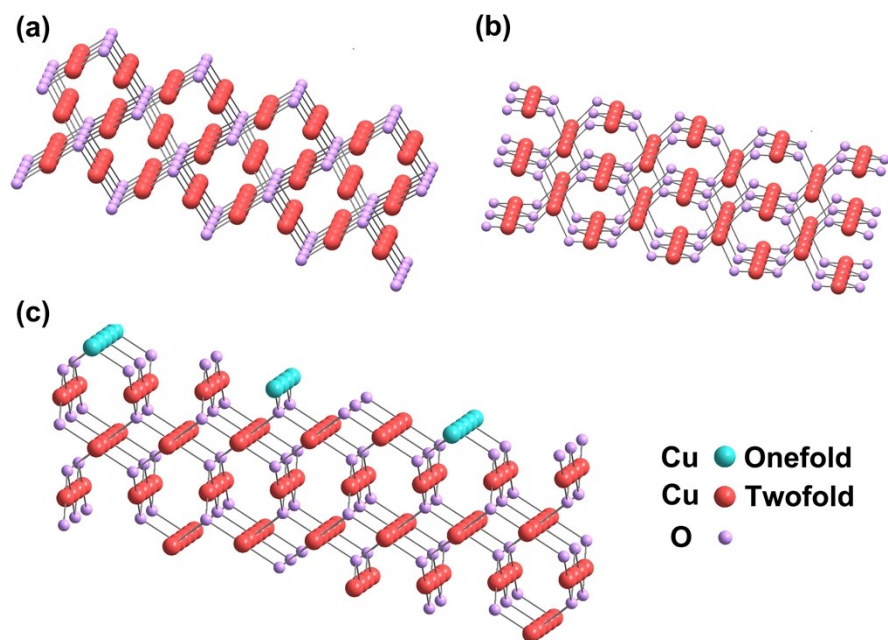


Fig. S14 Schematic models of (a) (100), (b) (110), and (c) (511) surfaces of Cu_2O .

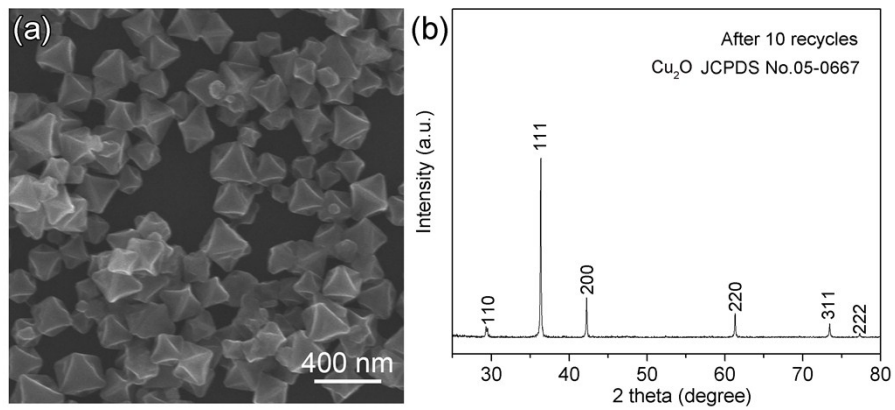


Fig. S15 (a) SEM image and (b) XRD pattern of truncated concave octahedral Cu_2O nanocrystals after 10 cycles of catalytic reaction.

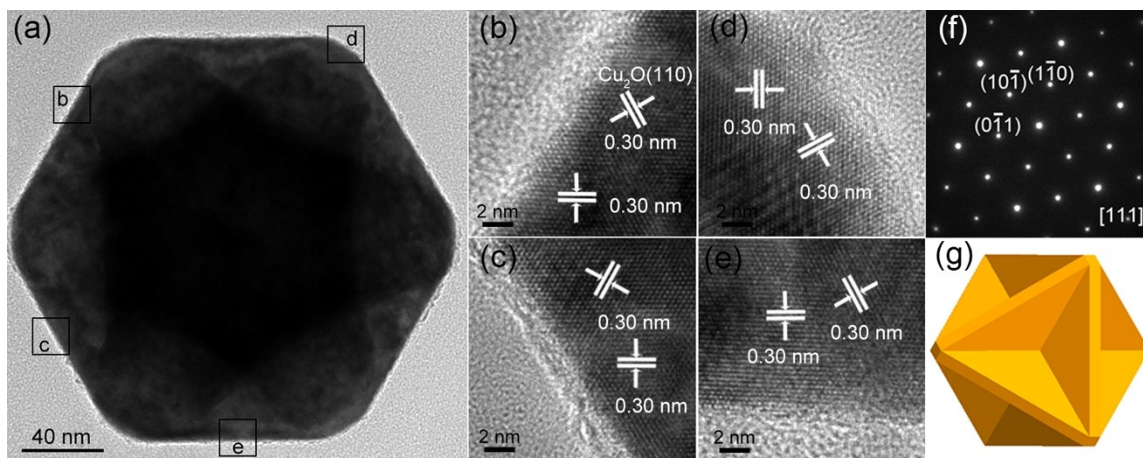


Fig. S16 (a) TEM, (b-e) HRTEM images, and (f) the corresponding SAED pattern of a truncated concave octahedral Cu_2O after 10 recycles of catalytic reaction. (g) Schematic model of a truncated concave octahedron viewed along $[111]$ direction.

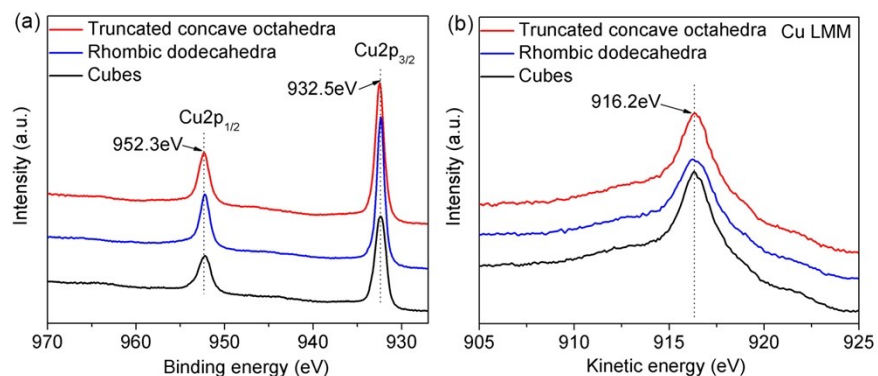


Fig. S17 (a) Cu 2p XPS and (b) Cu LMM Auger spectra of Cu₂O nanocrystals with different morphologies.

The surface copper oxidation states of three types of catalysts (truncated concave octahedra, rhombic dodecahedra, and cubes) were confirmed by XPS. As shown in Fig. S17a†, the peaks located at 932.5 and 952.3 eV can be attributed to Cu₂O. Cu LMM Auger spectra (Fig. S17b†) further showed that only Cu₂O Auger feature at 916.2 eV kinetic energy can be observed, and there is no existence of metallic Cu⁰ feature at 918.0 eV kinetic energy.^{3,4} These results demonstrated that the surface copper oxidation states of the three types of catalysts are +1.

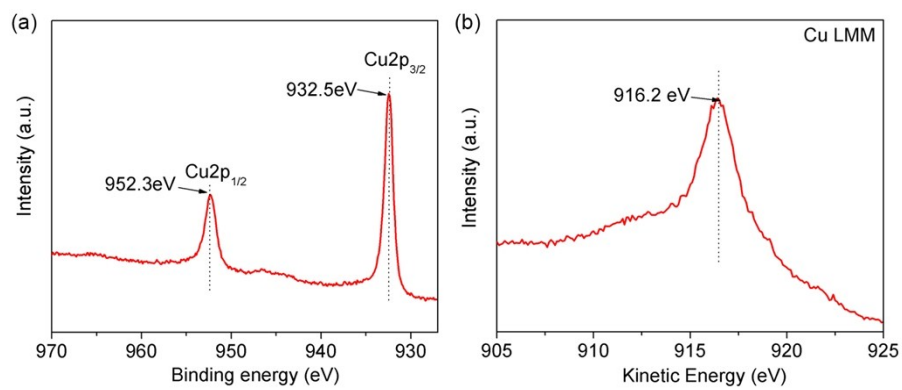


Fig. S18 (a) Cu 2p XPS spectra and (b) Cu LMM Auger spectra of truncated concave octahedral Cu_2O nanocrystals after 10 cycles of catalytic reaction.

Table S1 Comparison of catalytic parameters of Cu-based nanocatalysts in azide-alkyne cycloaddition reaction.

Catalysts	Azides (mmol)	Alkynes (mmol)	$\frac{m_{\text{catalyst}}}{m_{\text{alkyne}}}$	Conditions	Yields	TOF (h ⁻¹)	References
Fe/Cu NP	 (0.5)	 (0.6)	39.5%	1 mL H ₂ O, 0.25 mmol Et ₃ N, 2 wt.% TPGS-750-M room temperature (r.t.), 6 h	99%	-	5
Cu NP@montmorillonite	 (1)	 (1)	24.5%	10 mL H ₂ O, 1 mmol Et ₃ N, r.t., 1 h	95%	-	6
Cu NP-PEG@SBA-15	 (0.5)	 (0.5)	10.5%	2 mL H ₂ O, 35 °C, 24 h	100%	625	7
micelle-encapsulated Cu ₂ O particle	 (0.1)	 (0.1)	1.2%	0.5 mL H ₂ O, r.t., 24 h	99%	-	8
Cu ₂ O	 (1)	 (1.2)	14.1%	1 mL H ₂ O, r.t., 4 h	90%	-	9
Cu@Al ₂ O ₃	 (1) NaN ₃ (1)	 (1)	4	Ball-milling, r.t., 1 h	96%	-	10
Rhombic dodecahedral Cu ₂ O	 (0.25) NaN ₃ (0.38)	 (0.25)	8%	3 mL EtOH, 55 °C, 1 h	96%	6652	11
Octahedral Cu ₂ O	 (0.25) NaN ₃ (0.38)	 (0.25)	1.9%	3 mL EtOH, 55 °C, 2 h	98%	-	12
Truncated concave octahedral Cu ₂ O	 (0.25)	 (0.25)	7.7%	1 mL H ₂ O, 40 °C, 70 min	98%	2413	This work

Given the green reaction condition, when only using water as a solvent, truncated concave octahedral Cu₂O with the size of 158 nm in our work showed higher TOF (2413 h⁻¹) with 98% yield of target triazole, whereas other reported Cu-based nanocatalysts needed much longer reaction times to achieve high yields of target triazoles.

Although rhombic dodecahedral Cu_2O showed a high TOF value of 6652 h^{-1} (reference 11), organic solution (ethanol) was used as the solvent and the reaction was performed in a higher temperature ($55 \text{ }^\circ\text{C}$) relative to our system. In addition, rhombic dodecahedral Cu_2O nanocrystals can also be obtained in our work and truncated concave octahedral Cu_2O showed higher activity than rhombic dodecahedral Cu_2O .

Table S2 Calculated crystallite sizes (D) of different types of Cu_2O nanocrystals based on XRD using Scherrer equation.

Samples	D (nm)		
	(110)	(111)	(200)
Truncated concave octahedra	167	177	173
Rhombic dodecahedra	181	169	165
Cubes	178	179	150

The crystallite size (D) was calculated according to the Scherrer equation ($D = K\lambda/\beta \cos\theta$), where K is Scherrer's constant ($K = 0.89$), λ is the wave length of Cu $K\alpha$ radiation ($\lambda=1.5406 \text{ \AA}$), θ is the diffraction angles of the (110), (111), and (200) peaks of the Cu_2O crystals, and β is the full width at half-maximum (FWHM) of the corresponding (110), (111), and (200) peaks, after subtracting the instrumental line broadening. As shown in Table S2†, the calculated sizes of truncated concave octahedral, rhombic dodecahedral, and cubic Cu_2O nanocrystals are close to the measured sizes based on their SEM images.

Table S3 BET results for different types of Cu₂O nanocrystals.

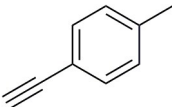
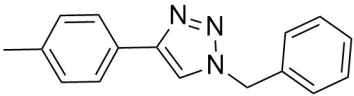
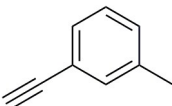
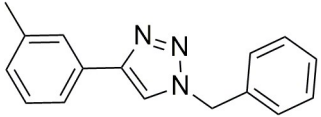
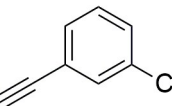
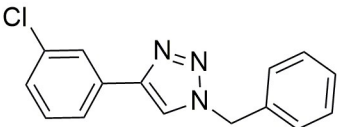
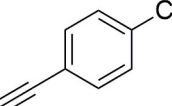
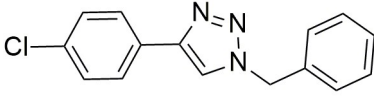
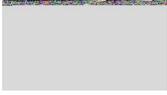
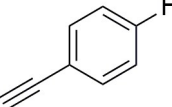
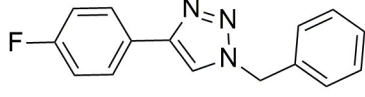
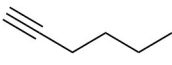
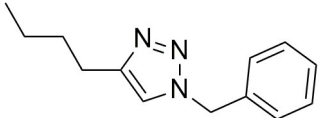
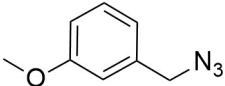
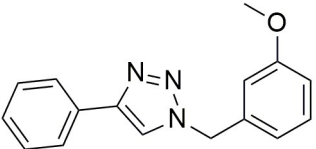
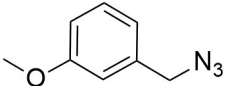
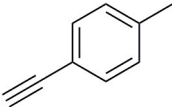
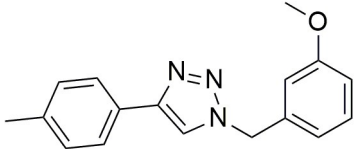
Samples	Specific surface areas (m² g⁻¹)
Truncated concave octahedra	6.58
Rhombic dodecahedra	6.00
Cubes	3.90

Table S4 The mole percentages of surface Cu(I) over the total Cu(I) in the Cu₂O catalysts.

Samples	Percentages of surface Cu(I) over the total Cu(I)^a
Truncated concave octahedra	0.399%
Rhombic dodecahedra	0.427%
Cubes	0.318%

^aThe percentages of surface Cu(I) over the total Cu(I) determined by CO-TPD

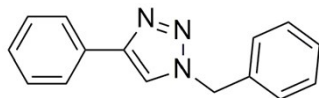
Table S5 Yields of different types of triazoles derived from the benzyl azide / benzyl azide derivative (0.25 mmol) and different types of alkynes (0.25 mmol) catalyzed by 2 mg (13.9 μ mol) truncated concave octahedral Cu₂O nanocrystals at 40 °C for 70 min.

Entry	Azides	Alkynes	Target products	Yield ^a , %
1				99 \pm 1
2				97 \pm 1
3				96 \pm 3
4				95 \pm 3
5				96 \pm 2
6				85 \pm 3
7				98 \pm 1
8				97 \pm 2

^aThe standard deviation based on three repeated experiments was given.

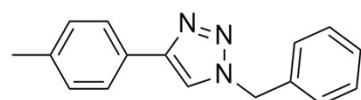
Spectral data of all synthesized compounds

1-Benzyl-4-phenyl-1*H*-1,2,3-triazole



^1H NMR (400 MHz, CDCl_3) δ 7.79 (d, $J = 8.2$ Hz, 2H), 7.66 (s, 1H), 7.40-7.36 (m, 5H), 7.32-7.28 (m, 3H), 5.55 (s, 2H); ^{13}C NMR (100 MHz, CDCl_3) δ 148.3, 134.8, 130.6, 129.2, 128.9, 128.8, 128.2, 128.1, 125.8, 119.6, 54.3.

1-Benzyl-4-(*p*-tolyl)-1*H*-1,2,3-triazole



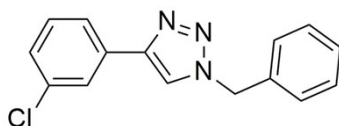
^1H NMR (400 MHz, CDCl_3) δ 7.68 (d, $J = 7.8$ Hz, 2H), 7.66 (s, 1H), 7.39-7.37 (m, 3H), 7.31-7.29 (m, 2H), 7.20 (d, $J = 7.8$ Hz, 2H), 5.56 (s, 2H), 2.36 (s, 3H); ^{13}C NMR (100 MHz, CDCl_3) δ 148.4, 138.1, 134.8, 129.6, 129.2, 128.9, 128.2, 127.9, 125.7, 119.2, 54.3, 21.4.

1-Benzyl-4-(*m*-tolyl)-1*H*-1,2,3-triazole



^1H NMR (400 MHz, CDCl_3) δ 7.65 (s, 2H), 7.56 (d, $J = 7.6$ Hz, 1H), 7.39-7.37 (m, 3H), 7.31-7.26 (m, 3H), 7.12 (d, $J = 7.2$ Hz, 1H), 5.57 (s, 2H), 2.38 (s, 3H); ^{13}C NMR (100 MHz, CDCl_3) δ 148.4, 138.6, 134.8, 130.5, 129.3, 129.1, 128.9, 128.2, 126.5, 122.9, 119.6, 54.3, 21.5.

1-Benzyl-4-(3-chlorophenyl)-1*H*-1,2,3-triazole



^1H NMR (400 MHz, CDCl_3) δ 7.77(m, 1H), 7.70 (s, 1H), 7.65-7.63 (m, 1H), 7.38-7.34 (m, 3H), 7.31-7.22 (m, 4H), 5.52 (s, 2H); ^{13}C NMR (100 MHz, CDCl_3) δ 146.8, 134.7, 134.5, 132.3, 130.1, 129.2, 128.8, 128.1, 125.7, 123.7, 120.1, 54.2.

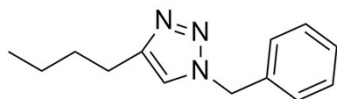
1-Benzyl-4-(4-chlorophenyl)-1*H*-1,2,3-triazole

¹H NMR (400 MHz, CDCl₃) δ 7.75 (d, *J* = 8.8 Hz, 2H), 7.65 (s, 1H), 7.41-7.36 (m, 5H), 7.32 (d, *J* = 5.2 Hz, 2H), 5.59 (s, 2H); ¹³C NMR (100 MHz, CDCl₃) δ 147.34, 134.6, 134.0, 129.4, 129.2, 129.0, 128.3, 127.1, 119.6, 54.4.

1-Benzyl-4-(4-fluorophenyl)-1*H*-1,2,3-triazole

¹H NMR (400 MHz, CDCl₃) δ 7.78-7.74 (m, 2H), 7.64 (s, 1H), 7.39-7.37 (m, 3H), 7.31-7.26 (m, 2H), 7.10-7.05(m, 2H), 5.56 (s, 2H); ¹³C NMR (100 MHz, CDCl₃) δ 163.9, 161.5, 147.4, 134.7, 129.3, 128.9, 128.2, 127.5, 127.4, 126.8, 119.4, 116.0, 115.8, 54.3.

1-Benzyl-4-butyl-1*H*-1,2,3-triazole



¹H NMR (400 MHz, CDCl₃) δ 7.39-7.32 (m, 3H), 7.27-7.24 (m, 2H), 7.19 (s, 1H), 5.49 (s, 2H), 2.69 (t, *J* = 7.8 Hz, 2H), 1.66-1.58 (m, 2H), 1.40-1.31 (m, 2H), 0.91(t, *J* = 7.4 Hz 3H); ¹³C NMR (100 MHz, CDCl₃) δ 149.0, 135.1, 129.1, 128.7, 128.0, 120.6, 54.0, 31.6, 25.5, 22.4, 13.9.

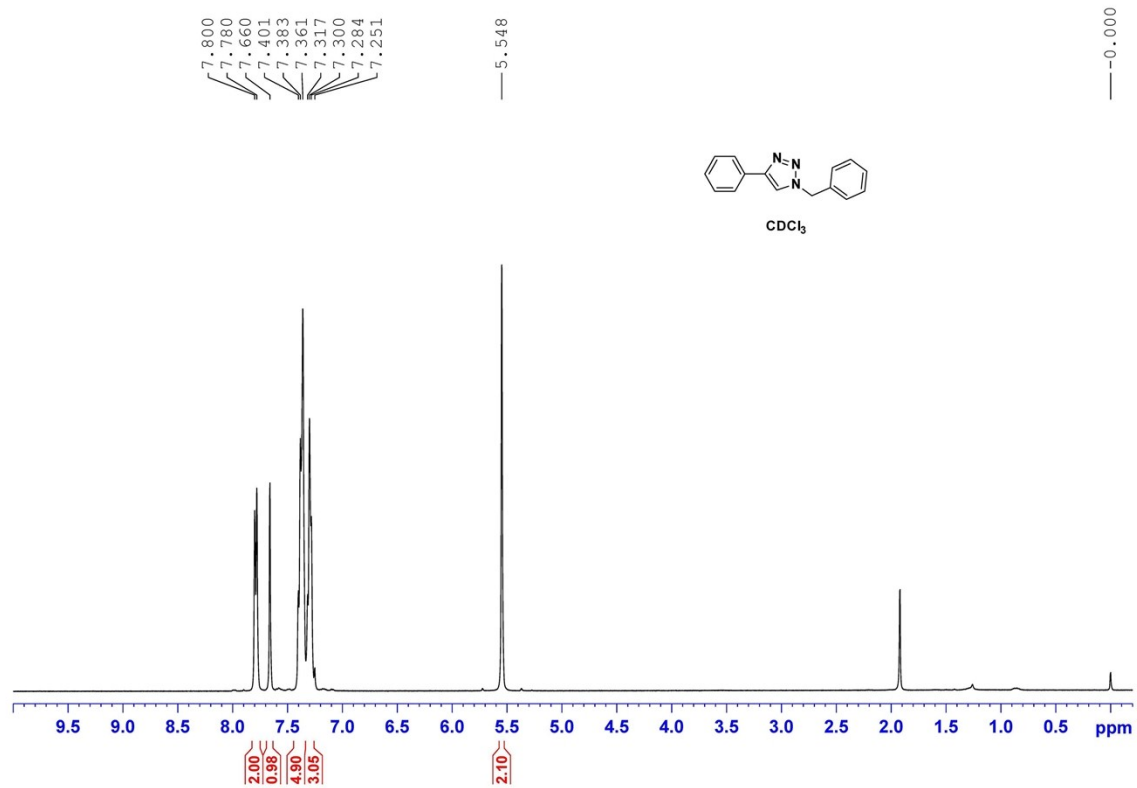
1-(3-methoxybenzyl)-4-phenyl-1*H*-1,2,3-triazole

¹H NMR (400 MHz, CDCl₃) δ 7.80 (d, *J* = 8.0, 2H), 7.68 (s, 1H), 7.40 (t, *J* = 7.6, 2H), 7.33-7.26 (m, 2H), 6.88(d, *J* = 7.8 Hz, 2H), 6.83(s, 1H), 5.53(s, 2H), 3.78(s, 3H); ¹³C NMR (100 MHz, CDCl₃) δ 160.2, 148.3, 136.2, 130.6, 130.3, 128.9, 128.3, 125.8, 120.3, 119.6, 114.3, 113.7, 55.4, 54.2.

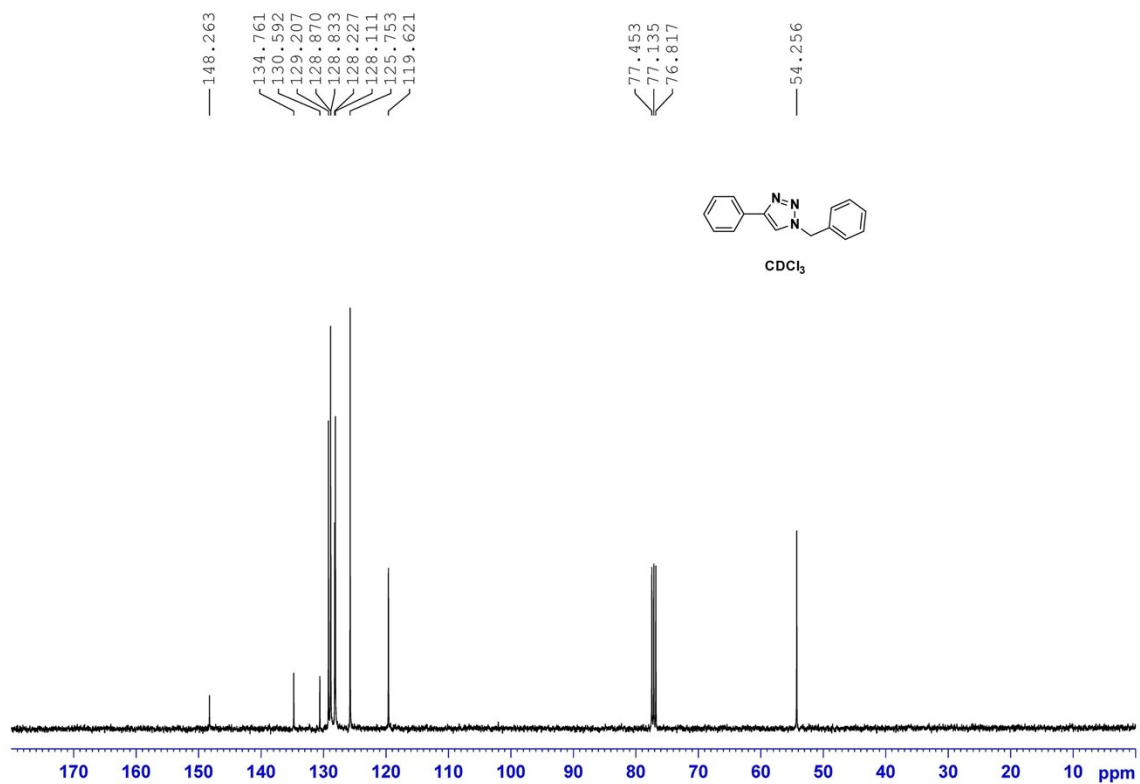
1-(3-methoxybenzyl)-4-(p-tolyl)-1*H*-1,2,3-triazole



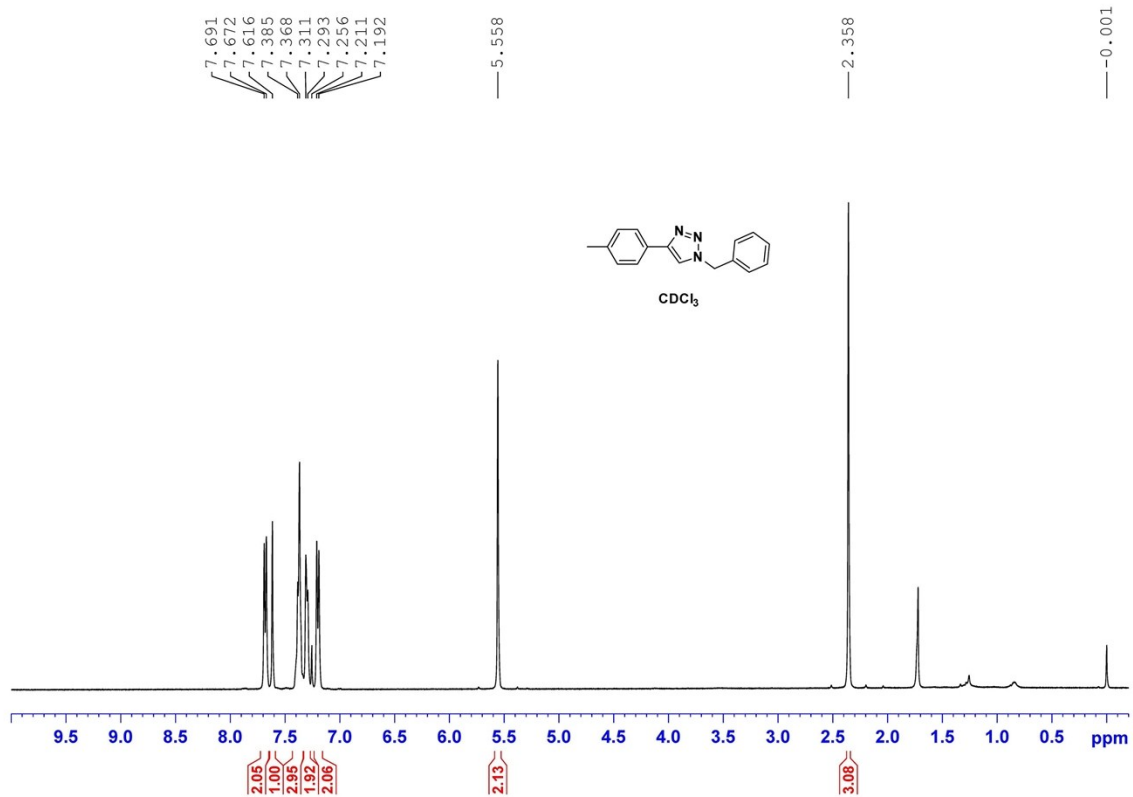
¹H NMR (400 MHz, CDCl₃) δ 7.67 (d, *J*=8.0, 2H), 7.63 (s, 1H), 7.27 (t, *J*=7.6, 1H), 7.19 (d, *J*=8, 2H), 6.87(d, *J* = 8 Hz, 2H), 6.81(s, 1H), 5.50(s, 2H), 3.78(s, 3H), 2.35(s, 3H); ¹³C NMR (100 MHz, CDCl₃) δ 160.1, 148.3, 138.0, 136.2, 130.3, 129.5, 127.7, 125.6, 120.3, 119.3, 114.2, 113.6, 55.4, 54.1, 21.4.



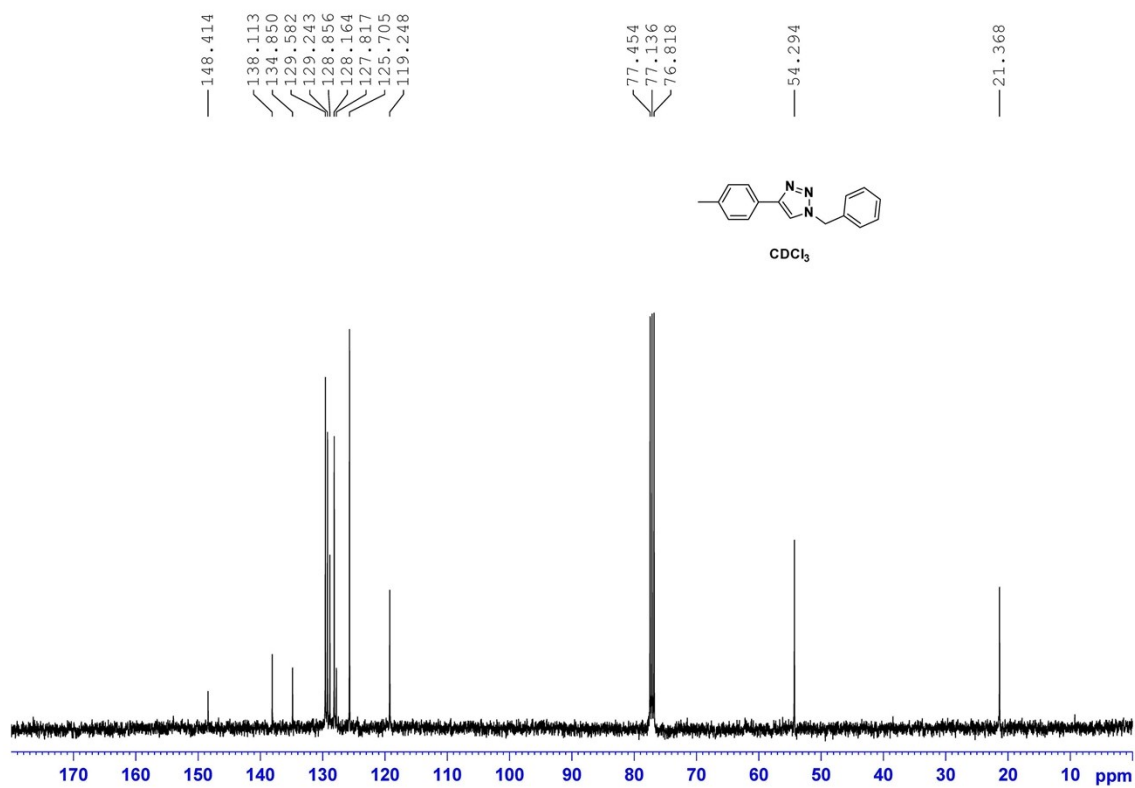
¹H NMR spectrum of 1-benzyl-4-phenyl-1H-1,2,3-triazole in CDCl₃ in 400 MHz



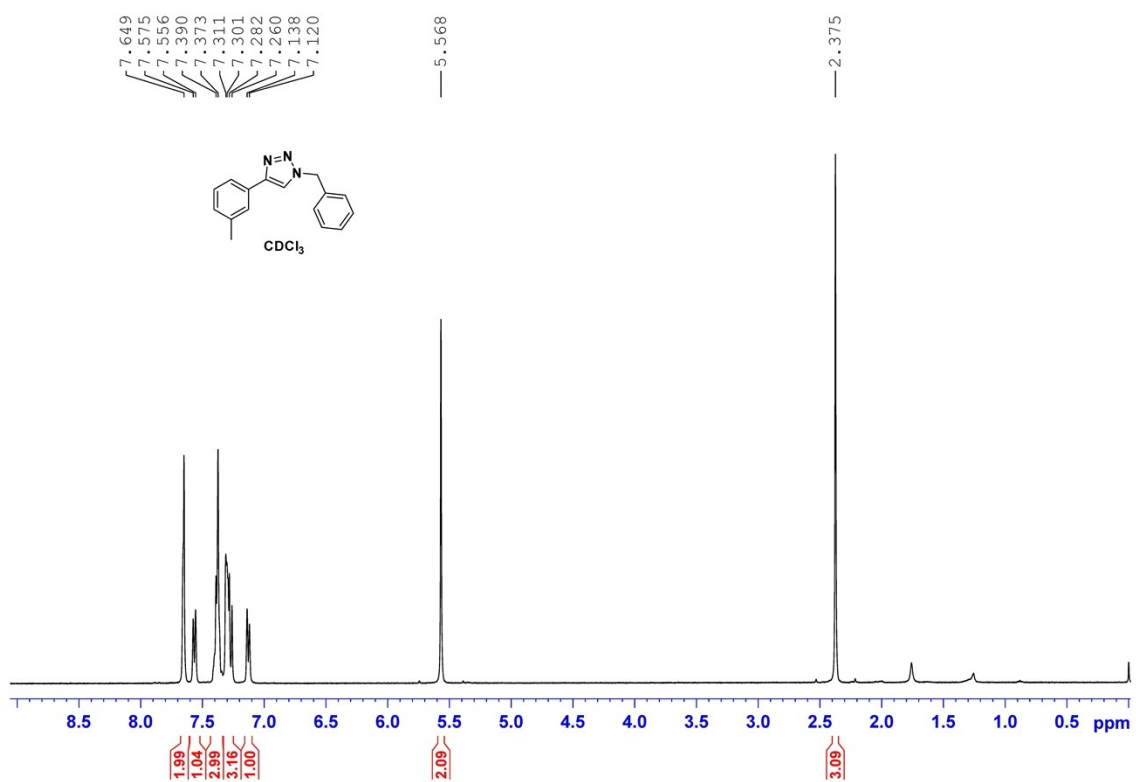
^{13}C NMR spectrum of 1-benzyl-4-phenyl-1H-1,2,3-triazole in CDCl_3 in 100 MHz



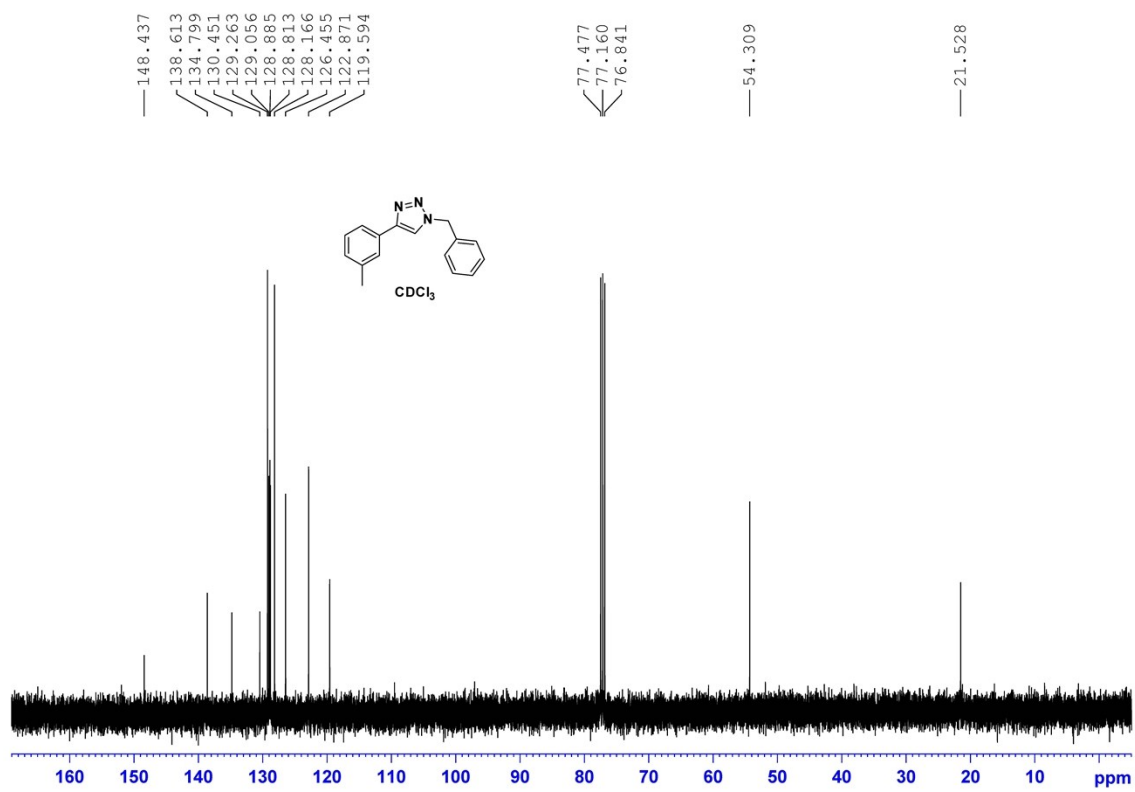
¹H NMR spectrum of 1-benzyl-4-(*p*-tolyl)-1*H*-1,2,3-triazole in CDCl₃ in 400 MHz



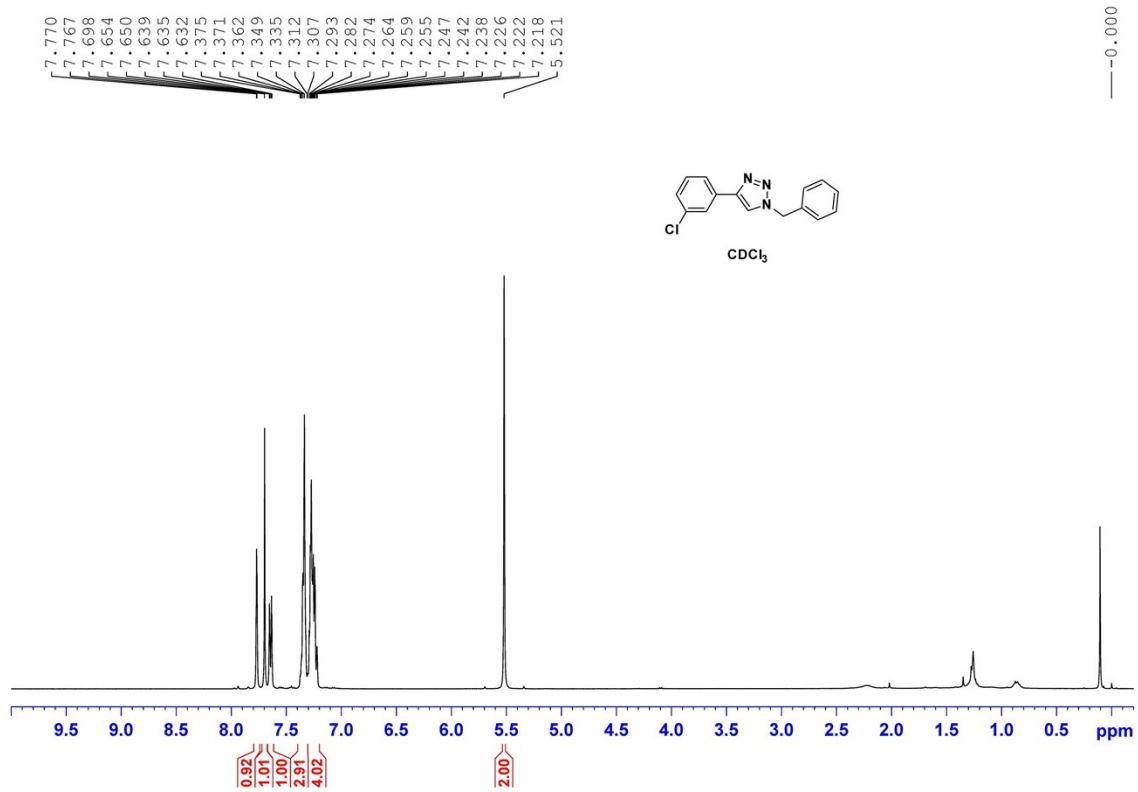
^{13}C NMR spectrum of 1-benzyl-4-(*p*-tolyl)-1*H*-1,2,3-triazole in CDCl_3 in 100 MHz



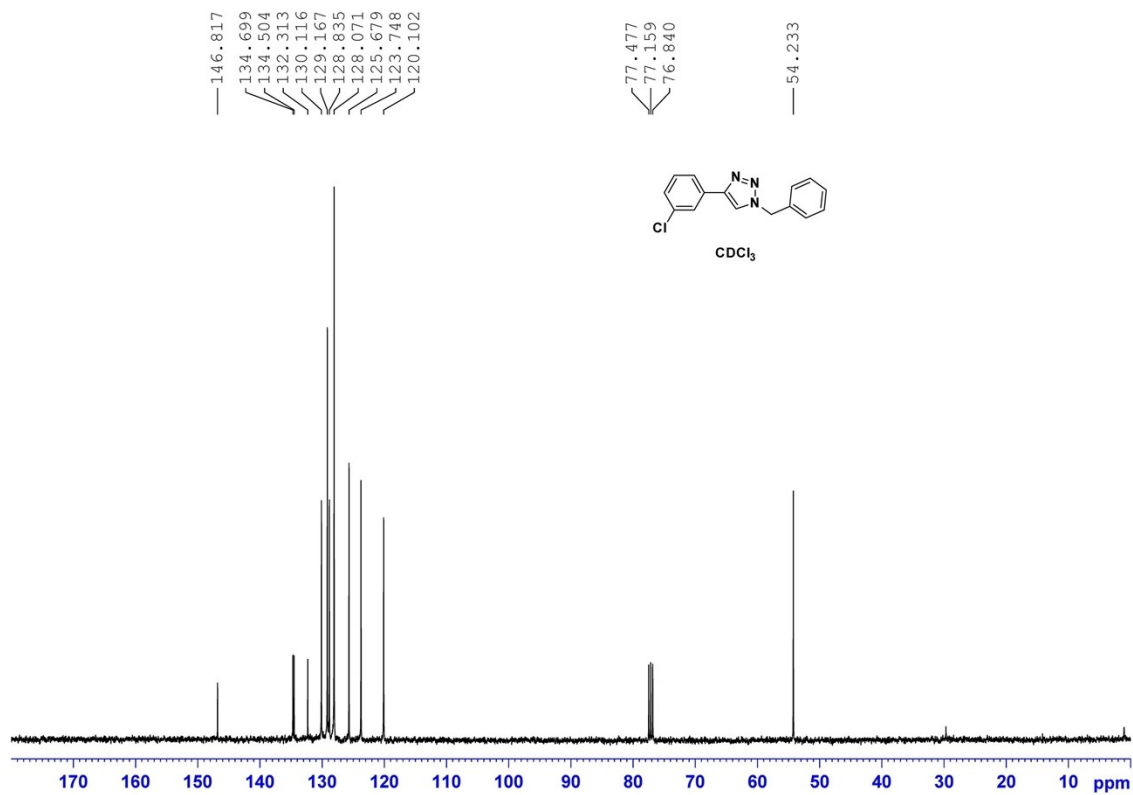
^1H NMR spectrum of 1-benzyl-4-(m-tolyl)-1H-1,2,3-triazole in CDCl_3 in 400 MHz



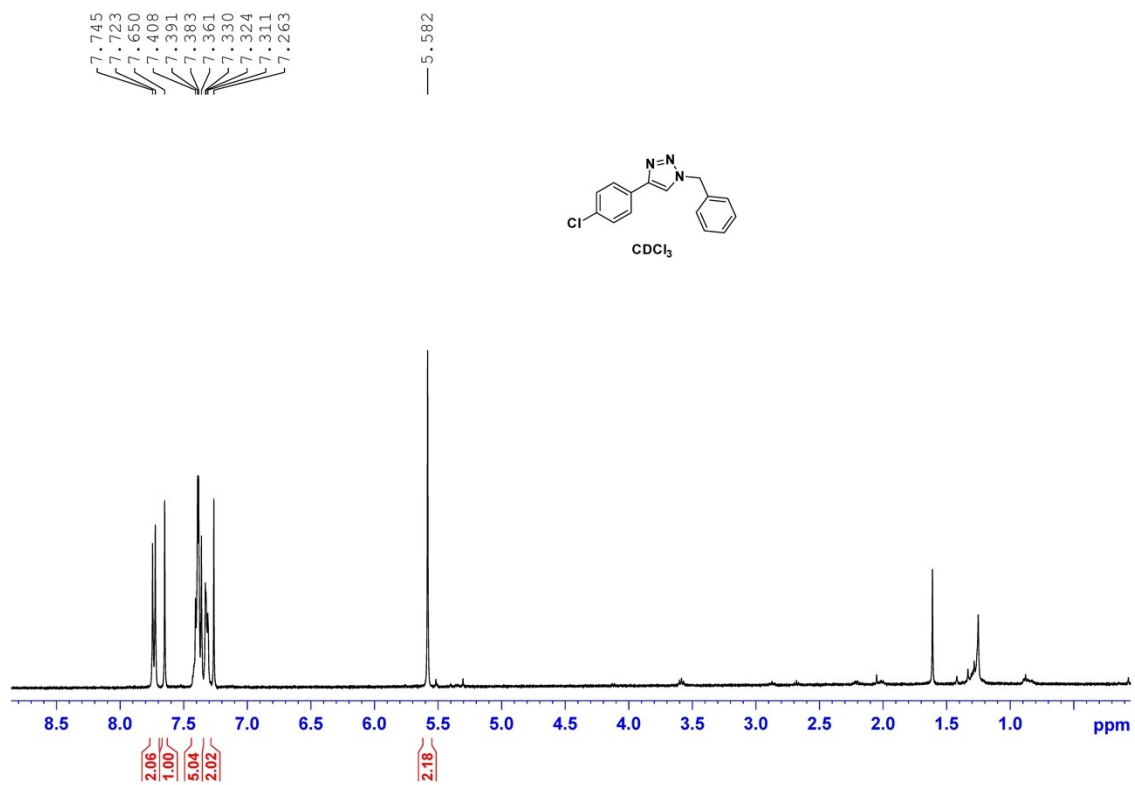
^{13}C NMR spectrum of 1-benzyl-4-(m-tolyl)-1H-1,2,3-triazole in CDCl_3 in 100 MHz



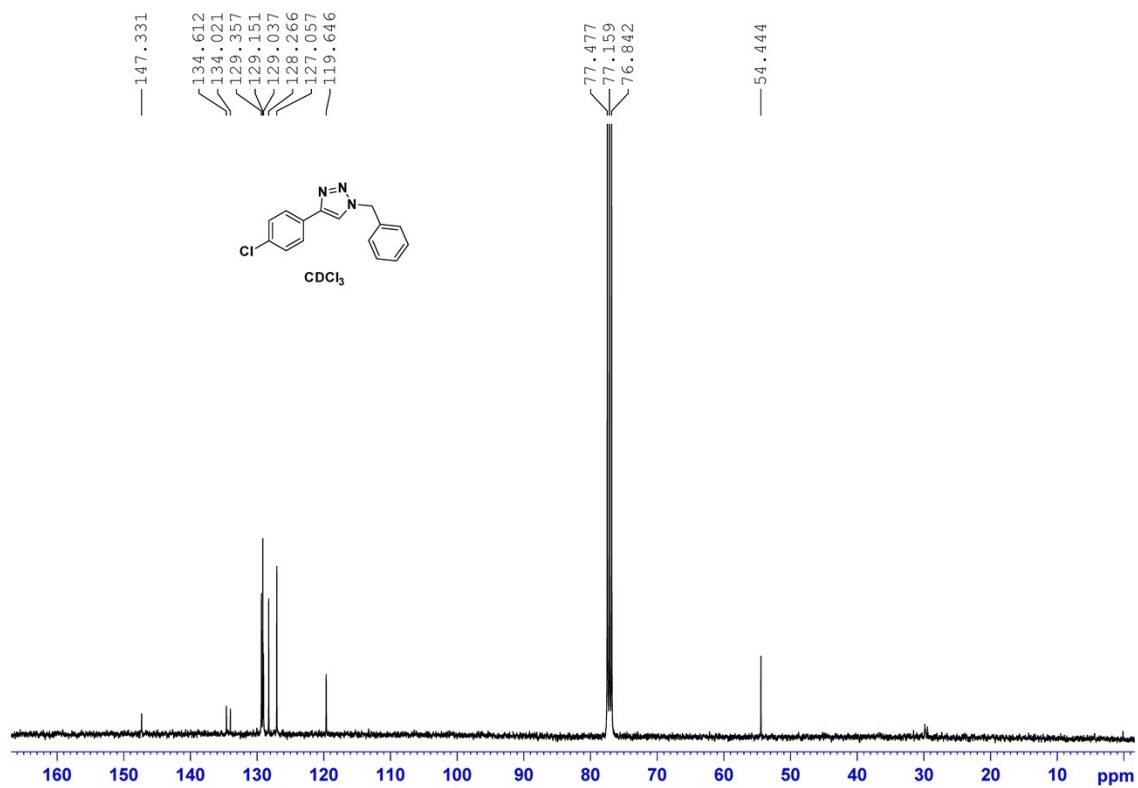
¹H NMR spectrum of 1-benzyl-4-(3-chlorophenyl)-1H-1,2,3-triazole in CDCl₃ in 400 MHz



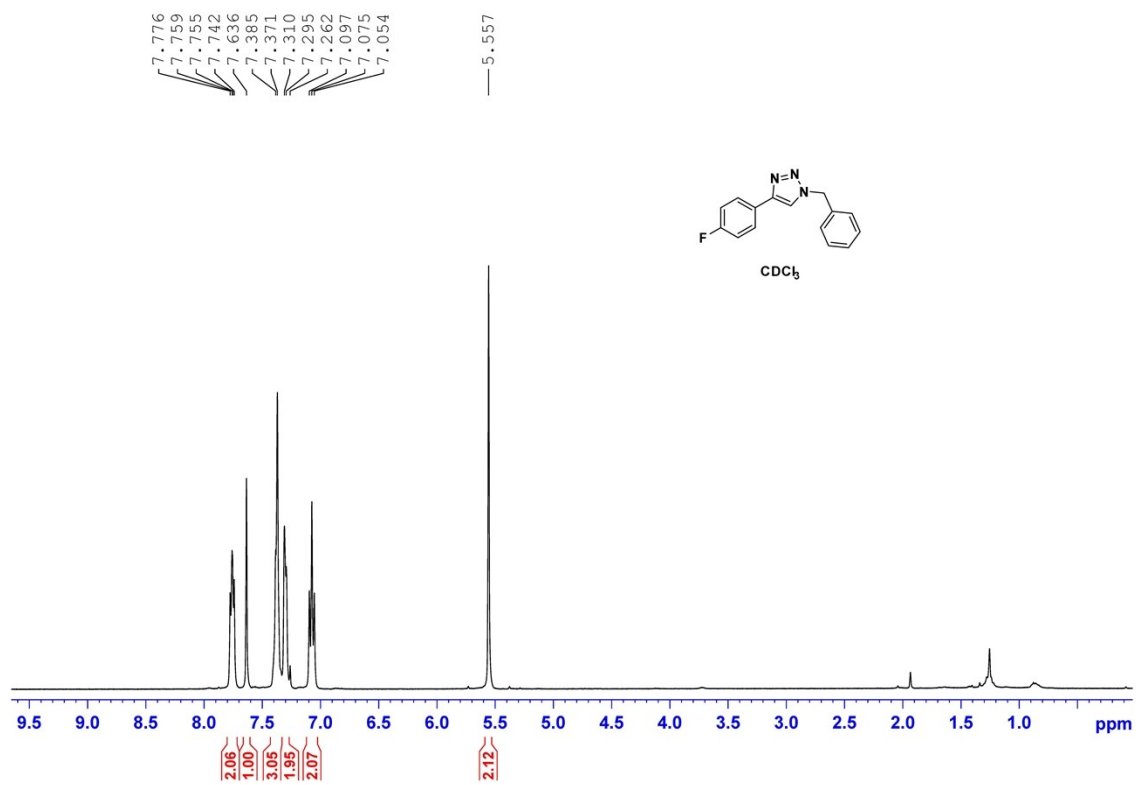
^{13}C NMR spectrum of 1-benzyl-4-(3-chlorophenyl)-1H-1,2,3-triazole in CDCl_3 in 100 MHz



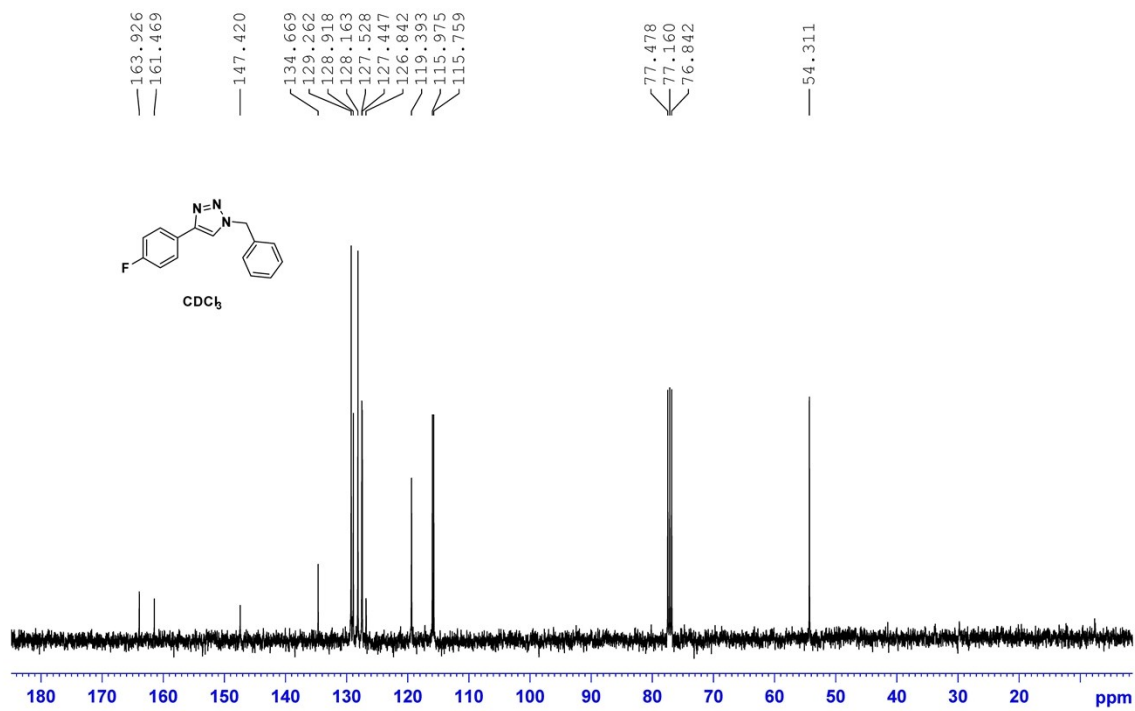
^1H NMR spectrum of 1-benzyl-4-(4-chlorophenyl)-1H-1,2,3-triazole in CDCl_3 in 400 MHz



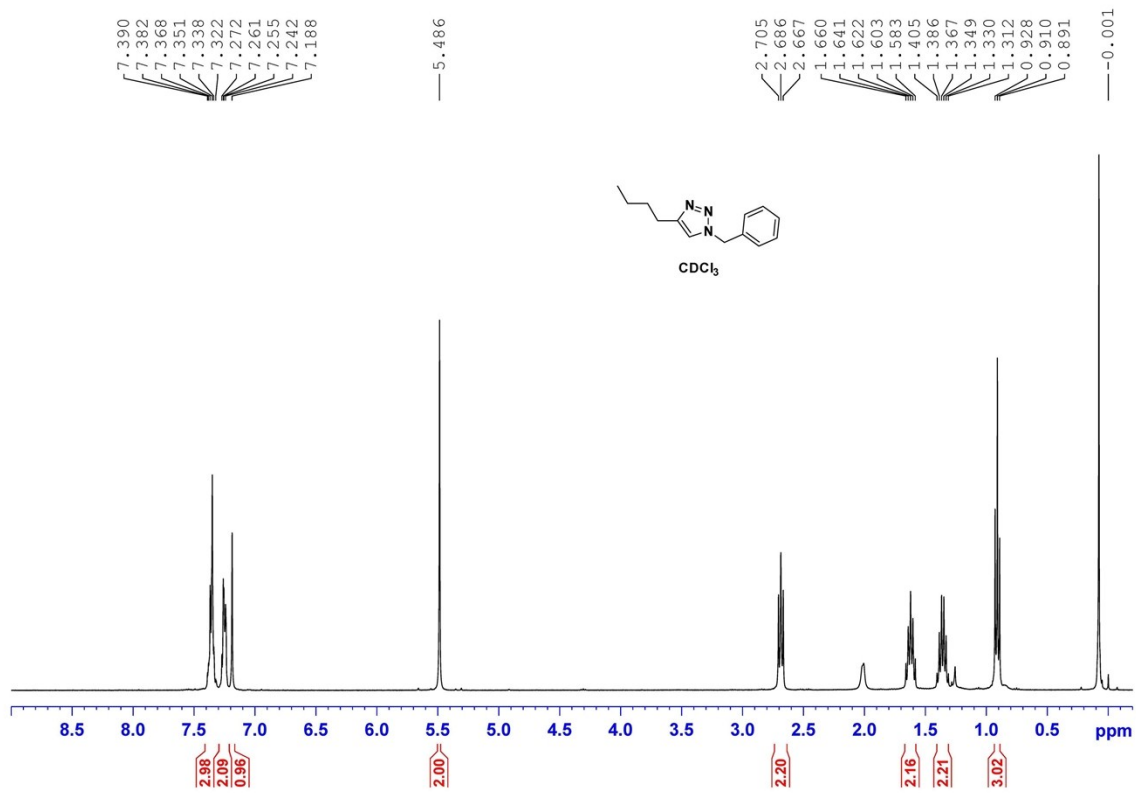
^{13}C NMR spectrum of 1-benzyl-4-(4-chlorophenyl)-1H-1,2,3-triazole in CDCl_3 in 100 MHz



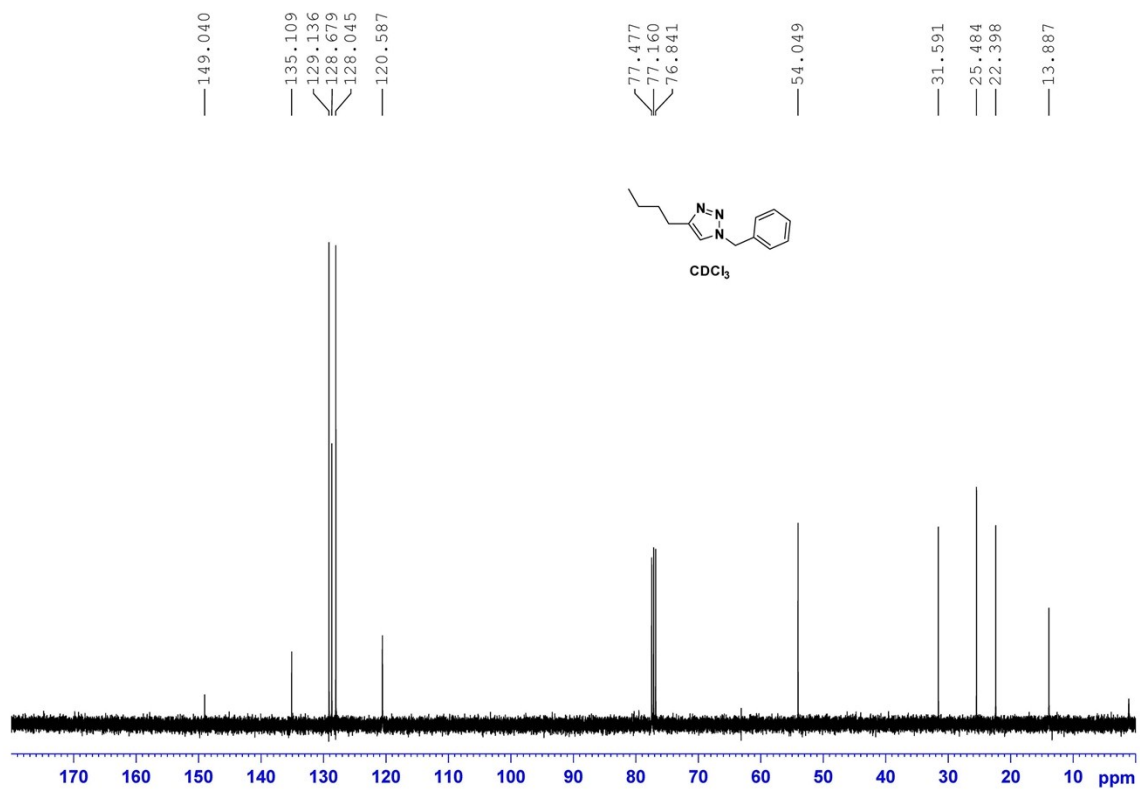
¹H NMR spectrum of 1-benzyl-4-(4-fluorophenyl)-1*H*-1,2,3-triazole in CDCl₃ in 400 MHz



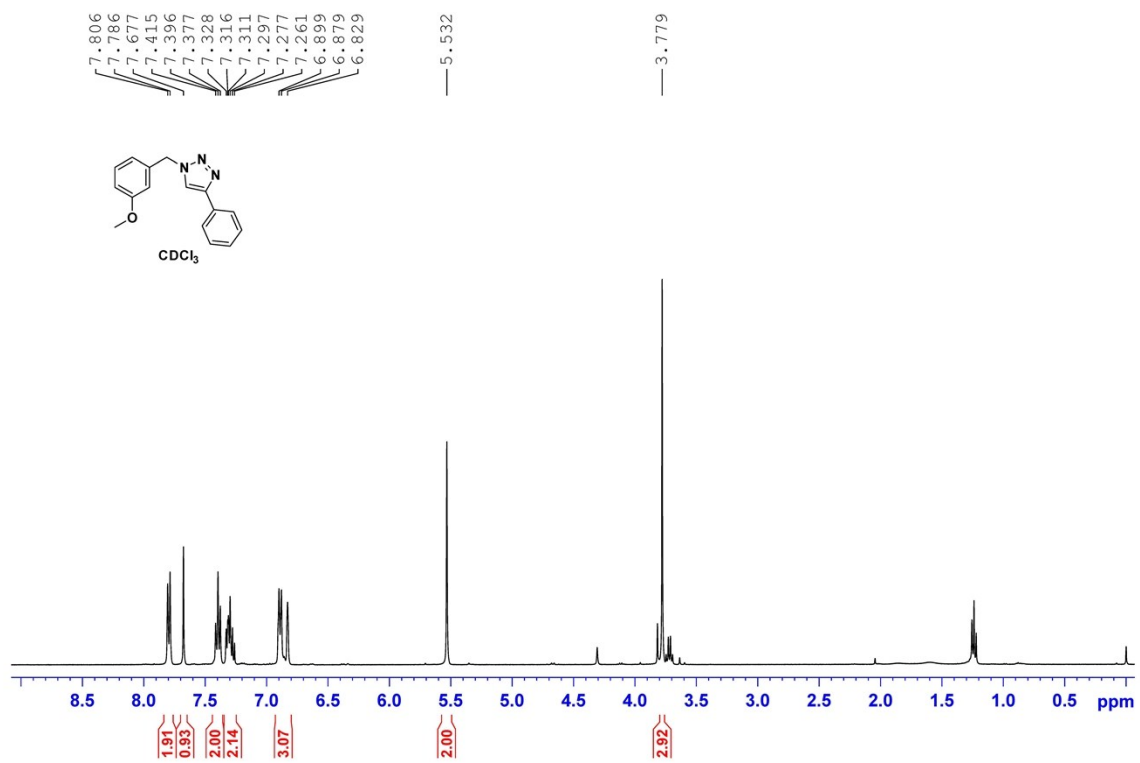
¹³C NMR spectrum of 1-benzyl-4-(4-fluorophenyl)-1H-1,2,3-triazole in CDCl₃ in 100 MHz



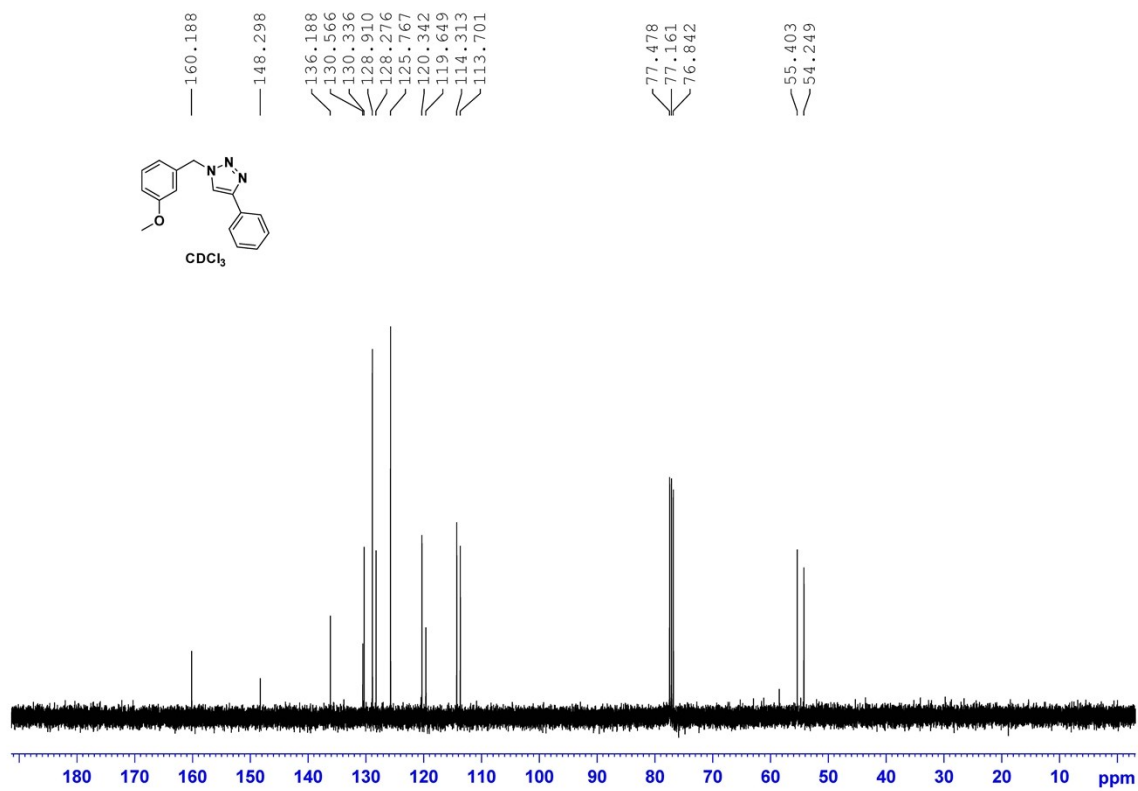
¹H NMR spectrum of 1-benzyl-4-butyl-1*H*-1,2,3-triazole in CDCl₃ in 400 MHz



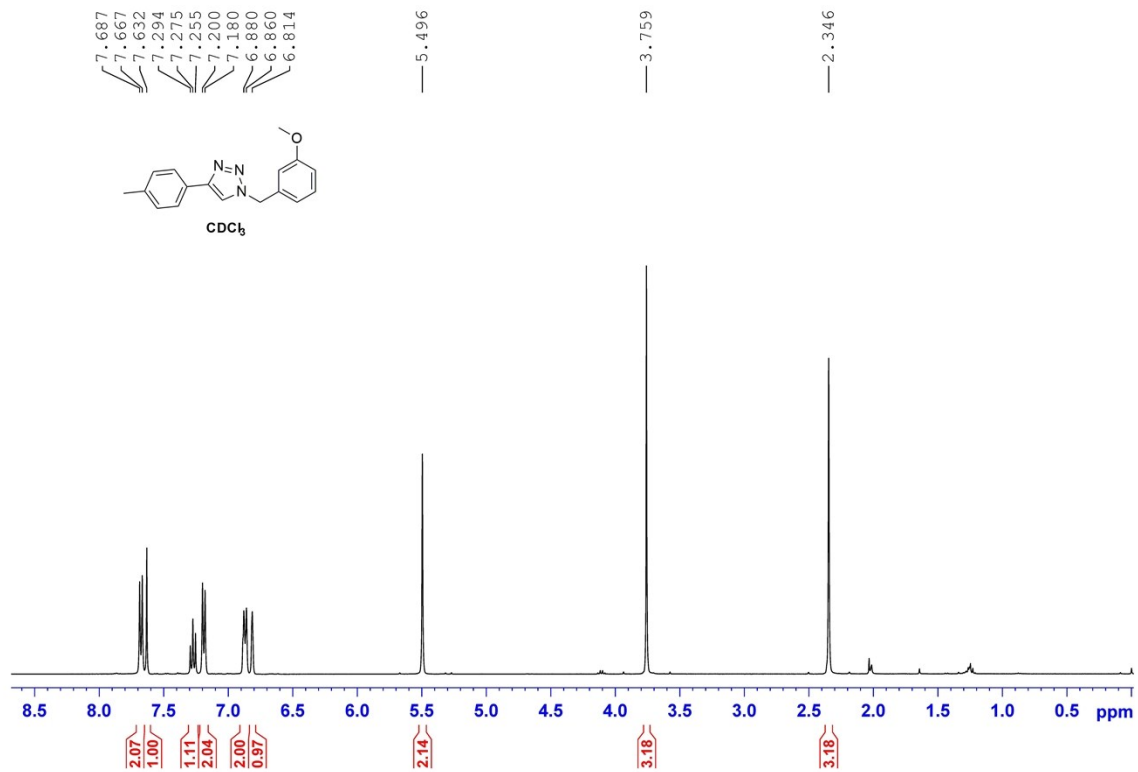
^{13}C NMR spectrum of 1-benzyl-4-butyl-1H-1,2,3-triazole in CDCl_3 in 100 MHz



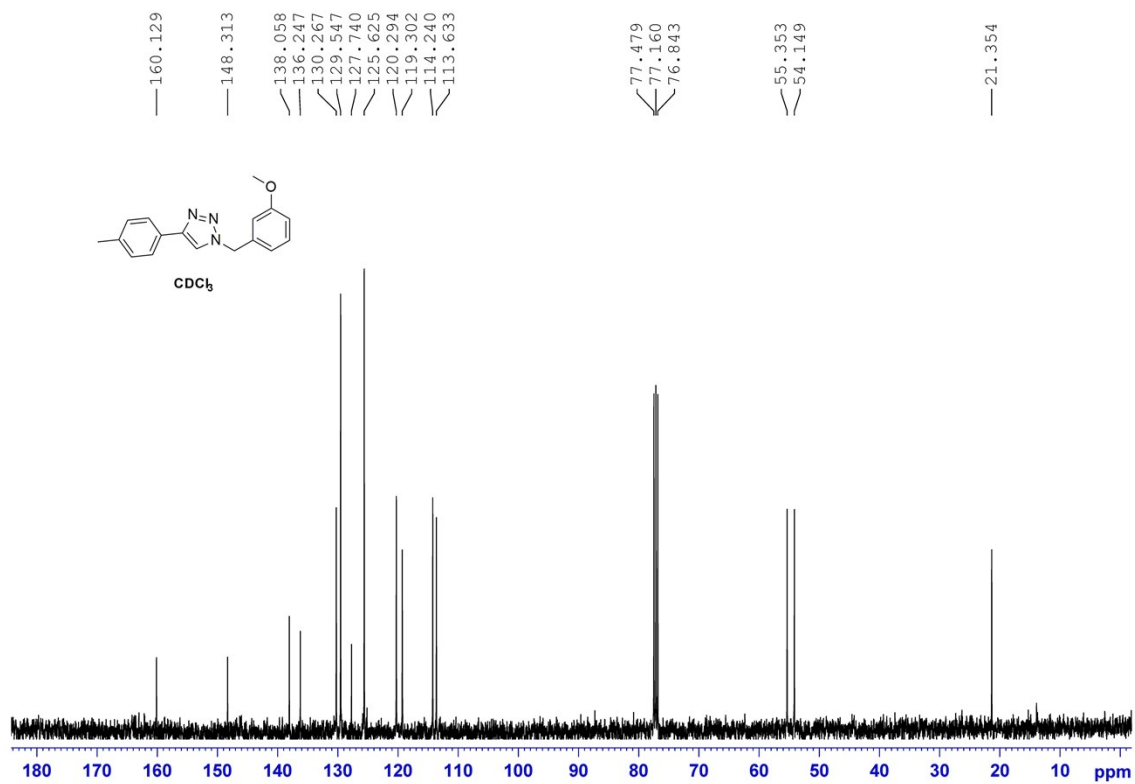
^1H NMR spectrum of 1-(3-methoxybenzyl)-4-phenyl-1*H*-1,2,3-triazole in CDCl_3 in 400 MHz



^{13}C NMR spectrum of 1-(3-methoxybenzyl)-4-phenyl-1*H*-1,2,3-triazole in CDCl_3 in 100 MHz



1H NMR spectrum of 1-(3-methoxybenzyl)-4-(p-tolylo)-1*H*-1,2,3-triazole in $CDCl_3$ in 400 MHz



¹³C NMR spectrum of 1-(3-methoxybenzyl)-4-(p-tolylo)-1H-1,2,3-triazole in CDCl₃ in 100 MHz